1 Introduction

Noise-induced hearing handicap in motorcyclists is a problem which is known to affect professional riders[1], in particular police officers[2, 3] and racing riders[4]. Previous studies of the causes and extent of such hearing damage have largely been motivated by the health and safety implications of hearing impairment and the resulting potential for litigation.

The precise mechanisms of hearing damage in motorcyclists are not yet clear, but it has been established [5] that noise levels at the ear of a rider can exceed $90\mathrm{dB(A)}$ at a speed of $50\mathrm{km/h}$ (30mph) and can reach $105\mathrm{dB(A)}$ at a speed of $112\mathrm{km/h}$ (70mph), the maximum speed limit on roads in the United Kingdom. Given such high noise exposures, it is no surprise that professional riders have been found to have hearing handicap ranging from 40% in racing riders to 6% in driving instructors [1], where hearing handicap is the percentage of the exposed population that will suffer a hearing loss of $30\mathrm{dB}$ or more.

The noise which affects motorcyclists is generated by flow on the helmet surface and propagates through the structure of the helmet and head. While there have been a number of studies which have measured the noise inside a helmet, few workers have studied the aerodynamics of helmets with respect to noise generation [6]. The work we report here is a first step towards a more detailed examination of the nature and mechanisms of noise generation and transmission in helmets.

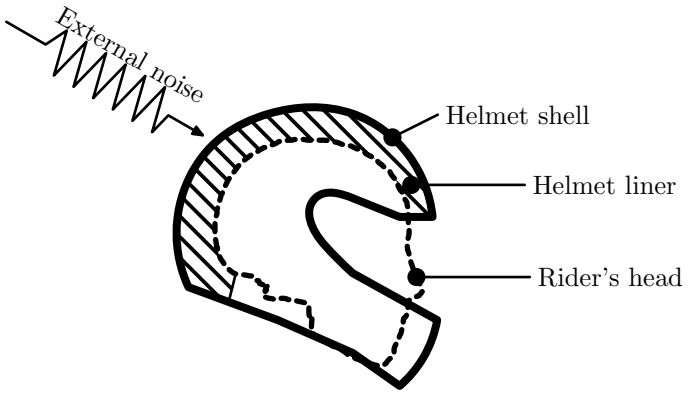

Figure 1: Model of the head-helmet acoustic system

2 Testing and data

Results are presented for tests carried out on UK public roads in June 2009. The test circuit was a six kilometre (3.5 miles) stretch of dual carriageway (maximum speed limit 70mile/h, $112\mathrm{km/h}$) between two roundabouts, ridden as a closed loop to give a total circuit length of $12\mathrm{km}$ (7 miles). The motorcycle used was a 2008 Suzuki GSXF-650 and the helmet a Shoei Raid II.

Instrumentation for the tests consisted of binaural microphones worn under the rider's helmet and an external pressure sensor placed at a number of different positions on the outside of the rider's

a *b* *c*

Figure 2: Sensor positions: *a*: pressure transducer positions on helmet shell; *b*: binaural microphones in place; *c*: pressure transducer mounted on shell in position 2.

helmet, Figure 2. Data were recorded on a Brüel and Kjaer SonoScout PDA-based acquisition system and sound level meter. A GPS unit gave reference data on motorcycle position and speed over the course of a test. Data were gathered over the whole circuit, each lasting fifteen to twenty minutes depending on traffic conditions. Traffic was free flowing and the only delays were due to queues at the roundabouts at each end of the test road. In the city, GPS signals occasionally dropped out going underground, such as when the motorcycle was near flyovers: such data were removed before processing.

2.1 Flow around helmets

The flow around motorcycle helmets in use on a motorcycle is not a problem which has attracted much attention in the open literature, although it is believed that the motorcycle proper, in particular the windscreen, has a large effect on the noise experienced by the rider [7]. Figure 3 shows images from wind tunnel tests conducted at the University of Bath by an undergraduate student a number of years ago. Smoke was used to visualize the low speed (approximately $10\mathrm{m/s}$) flow over a number of combinations of motorcycles and riders. These images show the flow over two well-established touring motorcycles, a BMW K1100 and Honda ST1100 Pan European. Due to differences in rider physiology and posture—a function of motorcycle design—and in windscreen geometry, the flow over the lip of the K1100 windscreen impinges on the rider's helmet near the chinbar and is deflected onto his chest. In the case of the ST1100, the flow impinges further up the helmet, in the region of the visor without the strong deflection onto the rider's chest.

If the helmet can be considered similar to a sphere in the flow, then it is possible to tentatively develop a crude model which should contain the essential features of our problem. Figure 4 shows such a model. It is assumed that the head can be represented by a sphere whose centreline is a distance h above the top of the windscreen, with h non-dimensionalized on sphere radius. The top of the windscreen sheds a vortex street which impinges on the sphere. For reference, the Reynolds number for a sphere of diameter $D = 300\mathrm{mm}$ at $80\mathrm{km/h}$ is $\mathrm{Re} = U_\infty D/\nu \approx 4.5 \times 10^5$

The dynamics of the problem are determined by the vortex shedding of the windscreen, by the

Figure 3: Flow over the windscreen of two different touring motorcycles: BMW K1100, left; Honda ST1100, right.

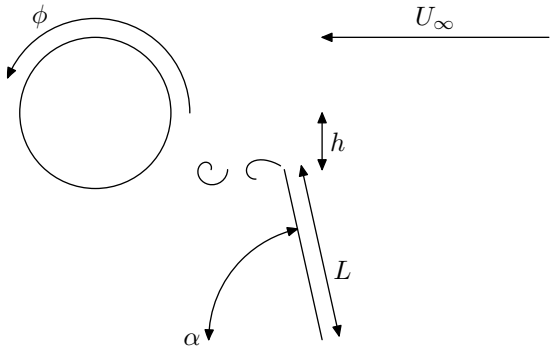

Figure 4: A crude model of flow over a helmet: L windscreen length; α windscreen inclination; h windscreen offset distance; U_∞ flow velocity.

flow over the sphere proper and by the evolution of the shed vortices from the windscreen as they interact with the sphere. Each of these is a major area of study in its own right but some general statements can be made. The boundary layer separation point for a smooth sphere at the indicated Reynolds number is at $\phi \approx 120^\circ$ from the inflow axis while the transition to turbulent flow occurs at $\phi \approx 95^\circ$ [8]. Given that a motorcycle helmet is not a smooth sphere in a uniform flow, we would expect both separation and transition to occur rather earlier but these figures are useful indications of what to expect. Certainly, we would expect the flow over the front of the helmet to be dominated by the effects of the windscreen. On the upstream side of a sphere, flow visualization studies at the relevant Reynolds numbers [9] show evidence of a vortex sheet shed from the back of the sphere to generate a vortex pair. For $\mathrm{Re} > 5 \times 10^5$, this feature oscillates randomly through less than 180°. We might expect to see such a feature in these tests, though probably at lower Reynolds number.

Secondly, there has been relatively little interest in vortex shedding from bodies similar to windscreens, such as flat plates at high incidence, but there are published data [10] which indicate that the Strouhal number for vortex shedding $\mathrm{St} = fL/U_\infty$ is independent of Reynolds number and roughly independent of incidence for $\alpha \gtrsim 60^\circ$, with $\mathrm{St} \approx 0.2$. At the level of fidelity adopted in the model, we assume that published results for the radiated noise from a body-vortex interaction are at least similar to the surface pressures generated by a sphere-vortex interaction. Such data are available [11, page 199] and do indeed show results of a type which we have found in the tests presented here.

2.2 Data processing

It has long been recognized that a turbulent flow, such as that responsible for the noise in motorcycle helmets, is characterized by the intermittent arrival of 'coherent structures' in the otherwise random fluctuations in the flow quantities. These coherent structures can be responsible for much of the noise generated by a flow and are not amenable to analysis by the traditional frequency domain, or spectral, approaches.

Here, we adopt the wavelet-based methods which have been used for some two decades to analyze the coherent part of turbulent flows [12–16]. The theory of wavelet transforms has been extensively described elsewhere but their essential feature is the ability to describe the content of a signal at different scales. For a function of some variable x, the discrete wavelet transform can be written in terms of a rescaled and translated 'mother function' Ψ_{00}:

$$\Psi_{kj}(x) = 2^{-k/2}\Psi_{00}(2^k x - j), \tag{1}$$

where k and j are integer indices so that a signal sampled on a discrete mesh $f(x_j)$, $x_j = j\Delta x$ can be written:

$$f(x_j) = \sum_{r=1}^{\infty}\sum_{i=-\infty}^{\infty} w^{(r)}(i)\Psi^{(r)}(i - 2^r j), \tag{2}$$

where r is a discretized scale $r_k = 2^{-k}$. The wavelet coefficients $w^{(r)}(i)$ are computed as:

$$w^{(r)}(i) = \sum_{j=-\infty}^{\infty} \Psi^r(i - 2^r j) f(j). \tag{3}$$

As a diagnostic for the detection of coherent structures in the flow, we use the local intermittency measure [14], LIM:

$$\mathrm{LIM}(r,i) = \frac{[w^{(r)}(i)]^2}{\langle [w^{(r)}(i)]^2 \rangle}, \tag{4}$$

which can be used to detect non-uniform distributions of energy. The quantity $[w^{(r)}(i)]^2$ can be considered equivalent to the energy contained in the signal at scale r at time i. Normalized on its mean value, it gives a measure which can be used to detect the signatures of potential coherent structures passing over the sensor.

These signatures can be extracted by using peaks in the LIM as a trigger for a conditional averaging procedure, which gives a time record of the signal produced by coherent structures in the flow [15]. The method works by first computing the wavelet transform of sections of the signal $f(i)$. In each of these sections, the LIM is then computed. A threshold value of LIM at some scale r is then set as $\alpha \mathrm{LIM}_{\max}$ where $\mathrm{LIM}_{\max}$ is the maximum value of LIM in the section and $0 < \alpha < 1$. Points in the signal where $\mathrm{LIM} > \alpha \mathrm{LIM}_{\max}$ are then found. For each of these points, a subsection g of the signal is extracted, $g(q) = f(i_0 + q)$, $-m \leq q \leq m$, where i_0 is the point where $\mathrm{LIM} > \alpha \mathrm{LIM}_{\max}$ and m is a user-defined value. The different realizations of g are averaged to give an estimate of the coherent structure signature. The result depends on α and on the scale r used for the LIM. In the results to be presented, α is varied to check for convergence of the educed signal. The resulting data have been found to be insensitive to r for the sampling parameters of these tests.

3 Results

The first set of results presented are the pressure sensor and microphone sensor spectra, shown in Figure 5. In the absence of a natural scaling length for the system, the results are shown as a function of $f/\bar{U}$, where f is frequency and U is vehicle speed. Results are shown for a 'high' speed, just less than the national speed limit, a 'middle' speed, typical of the highest speeds in urban areas, and 'low' speed, corresponding to the lowest standard speed limit on public roads. The motorcycle speed during the test for which data are presented is shown on each plot. The maximum value of $f/\bar{U}$ shown is $150\mathrm{m}^{-1}$, which corresponds to a frequency of $5\mathrm{kHz}$ at a speed of $120\mathrm{km/h}$. The first obvious point, reading down the columns of Figure 5 is the similarity of the 'high' and 'middle' speed results, when frequency is scaled on vehicle speed. The 'low' speed results on the other hand are quite different. We believe that this is because at low speed, the background noise from traffic and other environmental factors is comparable to the relatively weak aerodynamically generated noise from the helmet proper.

The second point to note is that while the measured external pressures are quite similar when the sensor is placed on the front or side of the helmet, the spectrum at the rear is very different, having a higher maximum value and a faster decay with frequency. This is as expected, on the basis of the aerodynamics of vortex shedding from spheres, given that the rear sensor position is behind the nominal separation point.

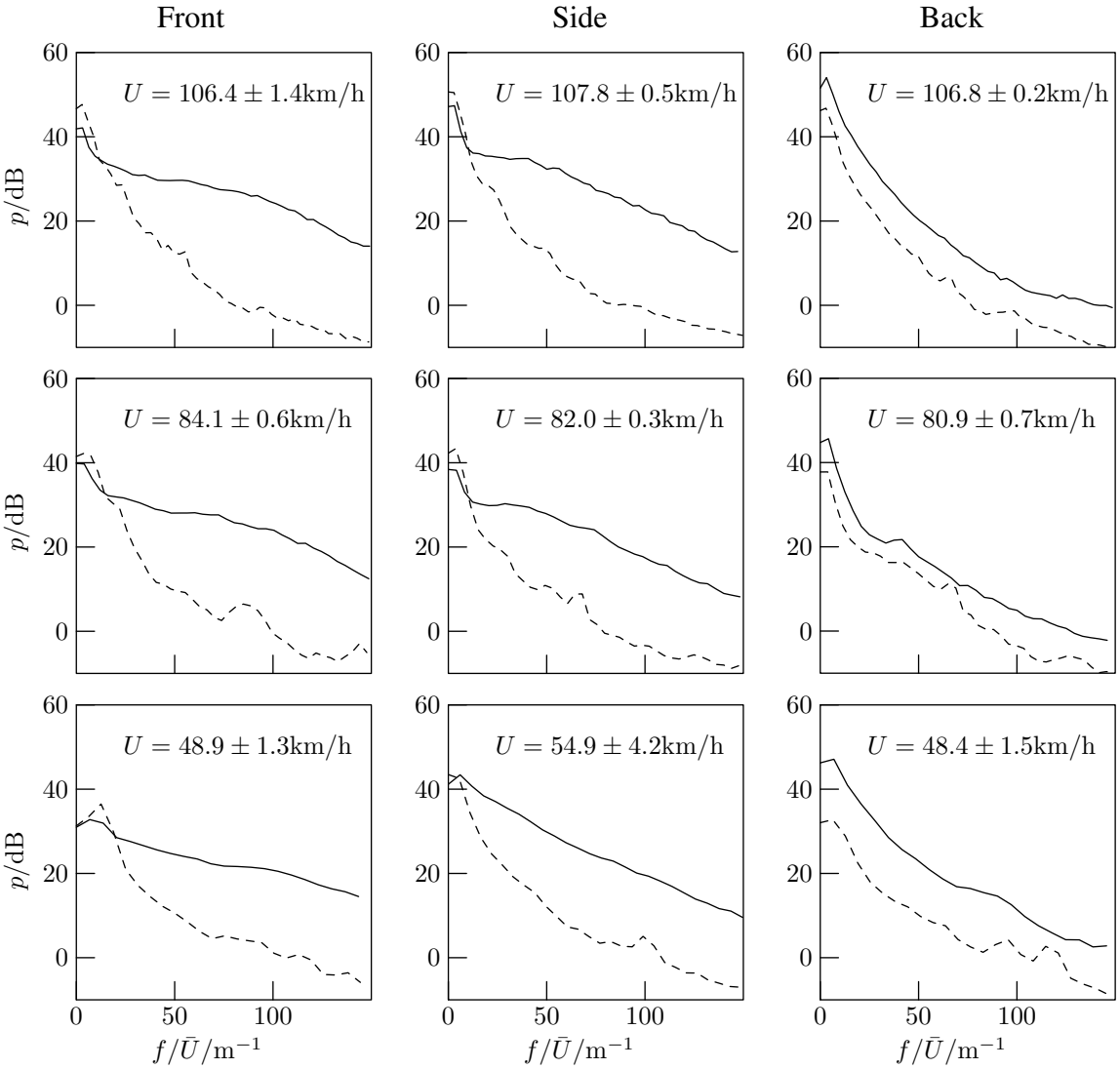

Figure 5: Spectra for pressure sensor (solid line) and internal microphone (dashed)

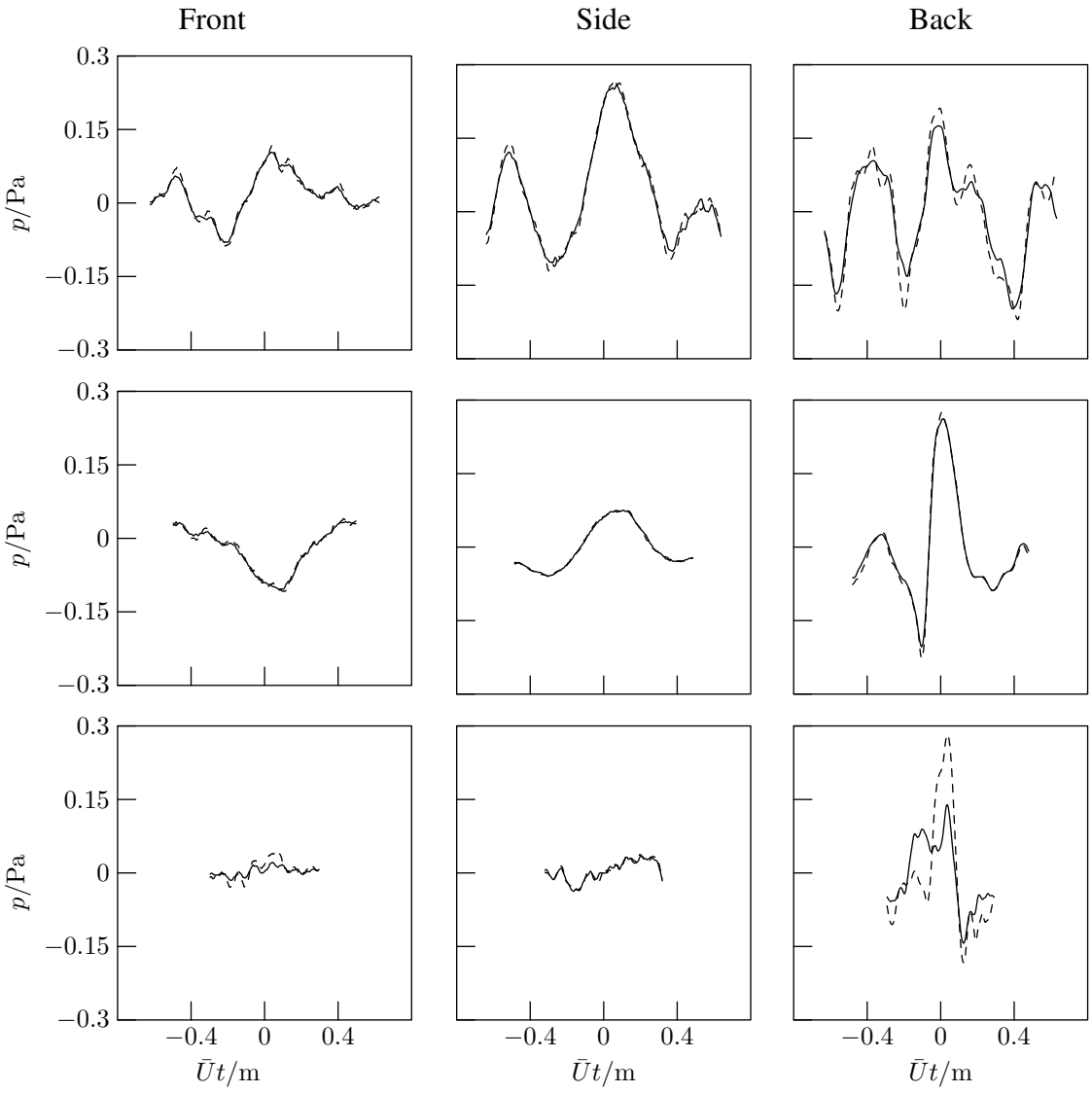

Figure 6: Educed coherent structures for the same cases as in Figure 5, solid and dashed lines show structures educed with two different thresholds for LIM.

Figure 6 shows the pressure signatures educed using the procedure of §2.2. The results are presented as pressure against $\bar{U}t$, to normalize the time scale. Also, the signals shown have been computed with two different values of the LIM threshold α. The difference between the two curves in each plot gives an indication of how well the estimated signal has converged.

Again, the 'low speed' data are quite different from the 'high' and 'middle' cases, with no well-defined structure being detected. This is to be expected since without a high enough forward speed, there is no well-defined mean flow or flow direction. In the case of the rear-mounted sensor at low speed, the educed structure has a large amplitude but with considerable variation between the signals educed at two different threshold levels, so that it cannot be considered a reliable estimate.

In the two higher speed cases, the educed structures vary a little in quality (e.g. the 'high speed' rear-mounted case), probably because of variation in the vehicle speed and inflow conditions over the duration of the data acquisition. The results must, then, be considered provisional until they can be replicated under better controlled conditions, but some tentative conclusions can be drawn.

With the exception of the low speed cases, and the possible exception of the side and rear high speed cases, the educed pressure signatures are well-defined, with the pressure falling off to zero at either end (so they can reasonably be called 'signatures') and with clear peaks.

Considering the 'middle' speed case, $\mathrm{Re} \approx 4.5 \times 10^5$, separation on a smooth sphere will happen at about 120° [8]. Even allowing for the effect of roughness and the non-spherical helmet, it is unlikely that separation will occur as far forward as the front sensor. The three pressure signals are consistent with a vortex filament passing over the helmet, deforming as it goes, while the rear signal may also be affected by the vortex structures generated by the sphere-alone flow.

In the 'high' speed case, any vortex structures shed by the windscreen will have larger circulation than in the lower speed cases and this will affect the amplitude of the measured pressures and also the dynamics of vortex interactions. The front-sensor signal is similar to its equivalent in the 'middle' speed case and may well also be generated by a similar flow interaction. The side and back signals are more problematic: the side signal is consistent with a strong vortex being accelerated past the sensor position but the back signal cannot be associated with a clearly-defined vortex-surface interaction. The side signal is well-converged, but the back signal still shows some variation between the estimates at two different thresholds, so that any interpretation based on this plot must be treated with care.

4 Conclusions

A set of data taken from on-road testing of noise and external aerodynamics of a motorcycle helmet have been presented. Using wavelet-based conditional averaging, the pressure signals of possible coherent structures in the flow have been educed. Based on these results, it is proposed that a large contribution to the noise-generating flow over the helmet is generated by vortex shedding from the motorcycle windscreen rather than by any factors intrinsic to a particular helmet. Future work will attempt to replicate these results with greater consistency and more detailed surface pressure measurements in a windtunnel.

Acknowledgements

The work presented in this paper has benefitted from the authors' membership of COST Action 357 PROHELM. We also wish to thank Mark Dowie and Paul 'Gunner' Weller of Brüel and Kjaer UK who supplied the measurement equipment and supported its use.

References

[1] Chris Jordan, Oliver Hetherington, Alan Woodside, and Harold Harvey. Noise induced hearing loss in occupational motorcyclists. *Journal of Environmental Health Research*, 3(2):70–77, 2004.

[2] M. C. Lower, D. W. Hurst, and A. Thomas. Noise levels and noise reduction under motorcycle helmets. In *Proceedings of Internoise 96*, pages 979–982, St Albans, 1996. Institute of Acoustics.

[3] M. C. Lower, D. W. Hurst, A. R. Claughton, and A. Thomas. Sources and levels of noise under motorcyclists' helmets. *Proceedings of the Institute of Acoustics*, 16(2):319–326, 1994.

[4] A. W. McCombe and J. Binnington. Hearing loss in Grand Prix motorcyclists: occupational hazard or sporting injury. *British Journal of Sports Medicine*, 28(1):35–37, 1994.

[5] B. C. Ross. Noise exposure of motorcyclists. *Annals of Occupational Hygiene*, 33(1):123–127, 1989.

[6] A. W. McCombe, J. Binnington, and D. Nash. Two solutions to the problem of noise exposure for motorcyclists. *Occupational Medicine*, 44:239–242, 1994.

[7] Jan Paul Peters. Private communication.

[8] Elmar Achenbach. Experiments on the flow past spheres at very high Reynolds numbers. *Journal of Fluid Mechanics*, 54(3):565–575, 1972.

[9] S. Taneda. Visual observations of the flow past a sphere at Reynolds numbers between 10^4 and 10^6. *Journal of Fluid Mechanics*, 85(1):187–192, 1978.

[10] Jerry M. Chen and Yuan-Cheng Fang. Strouhal numbers of inclined flat plates. *Journal of Wind Engineering and Industrial Aerodynamics*, 62:99–112, 1996.

[11] M. S. Howe. *Acoustics of fluid-structure interactions*. Cambridge University Press, 1998.

[12] Charles Meneveau. Analysis of turbulence in the orthonormal wavelet representation. *Journal of Fluid Mechanics*, 232:469–520, 1991.

[13] Charles Meneveau. Appendices A, B, & C to CTR manuscript 120. Technical report, Johns Hopkins University, Department of Mechanical Engineering, 1991. Available from Professor Meneveau.

[14] Marie Farge. Wavelet transforms and their applications to turbulence. *Annual Review of Fluid Mechanics*, 24:395–457, 1992.

[15] R. Camussi and G. Guj. Orthonormal wavelet decomposition of turbulent flows: intermittency and coherent structures. *Journal of Fluid Mechanics*, 348:177–199, 1997.

[16] Jori Ruppert-Felsot, Marie Farge, and Philippe Petitjeans. Wavelet tools to study intermittency: application to vortex bursting. *Journal of Fluid Mechanics*, 636:427–453, 2009.